J. Fluid Mech. (1989), *vol.* 206, *pp.* 375–404
Printed in Great Britain

Three-dimensionality of organized structures in a plane turbulent wake

By MICHIO HAYAKAWA[1] AND FAZLE HUSSAIN[2]

[1] Department of Mechanical Engineering II, Hokkaido University, Sapporo 060, Japan
[2] Department of Mechanical Engineering, University of Houston, Houston, TX 77004, USA

(Received 15 March 1988 and in revised form 8 March 1989)

This paper describes a quantitative study of the three-dimensional nature of organized motions in a turbulent plane wake. Coherent structures are detected from the instantaneous, spatially phase-correlated vorticity field using certain criteria based on size, strength and geometry of vortical structures. With several combinations of X-wire rakes, vorticity distributions in the spanwise and transverse planes are measured in the intermediate region ($10d \leqslant x \leqslant 40d$) of the plane turbulent wake of a circular cylinder at a Reynolds number of 13000 based on the cylinder diameter d. Spatial correlations of smoothed vorticity signals as well as phase-aligned ensemble-averaged vorticity maps over structure cross-sections yield a quantitative measure of the spatial coherence and geometry of organized structures in the fully turbulent field. The data demonstrate that the organized structures in the nominally two-dimensional wake exhibit significant three-dimensionality even in the near field. Using instantaneous velocity and vorticity maps as well as correlations of vorticity distributions in different planes, some topological features of the dominant coherent structures in a plane wake are inferred.

1. Introduction

In our previous experimental work (Hayakawa & Hussain 1985; Hussain & Hayakawa 1987, the latter being referenced hereinafter as HH), we developed a new technique for the study of organized motions (popularly called 'coherent structures') in turbulent shear flows, succeeded in employing it to map out the temporal evolution of the large-scale spanwise vorticity field, inferred the topology of the dominant coherent structure, and quantitatively evaluated the dynamical roles of the structure. This generic and robust technique which can in principle be applied to educe organized structures in any turbulent shear flow, recognizes spatially phase-correlated (i.e. coherent) motions underlying an apparently random turbulent flow from instantaneous vorticity maps without the use of any external signal for phase reference of trigger, and aligns and ensemble-averages different realizations to extract coherent and incoherent turbulence properties over the spatial extent of coherent structures. Being based on the vorticity field in a turbulent flow, the eduction algorithm can be applied to data obtained by any measurement technique as well as to data obtained by numerical simulation (e.g. Metcalfe *et al.* 1987*a*).

In the HH experiment, a rake of eight equally spaced X-wires was employed in the intermediate region of a cylinder wake, and the education was based on the spanwise vorticity field. The data revealed that there is increasing dispersion in individual vortex size, strength and displacement with increasing downstream distance; this dispersion occurs much sooner in the streamwise direction and is considerably more

prevalent than was previously suspected. In addition, the data disclosed the relative roles of saddles and centres and reaffirmed earlier experimental findings (Hussain 1980; Hussain & Zaman 1981; Cantwell & Coles 1983; Coles 1984) that the saddle region plays a crucial role in turbulence production. This result strongly suggests that the braid, connecting successive nominally spanwise vortical structures (i.e. rolls), consists of intermediate-scale coherent substructures (i.e. ribs) which are dominated by longitudinal vorticity and appear to be central to the turbulence production mechanism (Hussain 1984).

Led by these results along with our experiment and numerical simulation of a plane mixing layer (Metcalfe *et al.* 1987*a*), we concluded that longitudinal vortices and turbulence production by vortex stretching are characteristic features of all turbulent shear flows (Hussain 1984, 1986). An incidental consequence of this is that coherent structures contain regions of significant helicity (defined in the frame of a structure) even though locations of peak helicity and dissipation would not coincide (Hussain 1986). The rib structures have been observed in a number of visualization studies in plane mixing layers (Jimenez, Cogollas & Bernal 1985; Bernal & Roshko 1986; Lasheras, Cho & Maxworthy 1986) and have been presumed to play a substantial role in turbulence mixing. However, the dynamical roles of the ribs remain to be explored through quantitative measurements. These longitudinal structures must induce spanwise contortion of the spanwise rolls as demonstrated by direct numerical simulations (Grinstein, Oran & Hussain 1987; Metcalfe *et al.* 1987*b*), even though the strong two-dimensionality of the rolls has been claimed on the basis of flow visualizations (Brown & Roshko 1974; Breidenthal 1980) and hot-wire measurements of structure footprints (Wygnanski *et al.* 1979; Browand & Troutt 1985).

Historically, looking back to the studies of a cylinder wake, an early visual observation by Taneda (1959) revealed that the breakdown of the shed vortices occurred within about 100 diameters downstream from the cylinder and that organized smoke patterns, much like the Kármán vortex street but of a larger scale, reappeared farther downstream. He vaguely suggested that the formation of this new structure should be due to a hydrodynamic instability process. The rearrangement of the primary vortex street into new structure has been recently examined in further detail by several workers. Matsui & Okude (1981) suggested that vortex pairing was responsible for the change of structure spacing downstream, at least for Reynolds numbers lower than 160. Cimbala, Nagib & Roshko (1988) resurrected instability as the relevant mechanism (see also Wygnanski, Champagne & Marasli 1986). Parenthetically, we have cast strong doubt on the relevance of such an analysis based on the mean flow in highly turbulent fields which are dominated by large-scale structures at time- and lengthscales comparable with those of the instability mode (Hussain 1983, 1986).

Quite a different picture of the far-field structure in the wake had been proposed much earlier by Townsend (1956): the so-called 'double-roller eddies'. This structural module was reaffirmed (although revised) by the extensive correlation measurements of Grant (1958). The Grant model consists of paired counter-rotating eddies, perpendicular to the wake centreplane and accompanied by outward 'mixing jets' or entraining eddies. More recently, Townsend (1979) showed from multisensor measurements of the velocity field that large-scale velocity patterns in the wake had a fairly simple form with a distinct periodicity, although they appeared to be very complex owing to the superposition of patterns from eddies at all stages of the 'growth–decay–renewal cycle'. In a follow-up experiment, Mumford (1983) showed

the predominance of inclined double-roller eddies of several modes; some were confined to one side of the wake centreplane, while some extended across the centreplane, and even single-roller eddies were found. A possibility that the two roller structures on the two halves of a wake might be parts of a vortex loop connecting structures across the wake centreplane has been suggested by many (for example, Roshko 1976; Coles 1982; Savill 1983). However, this apparently plausible view remains speculative and needs to be examined by careful quantitative measurements or numerical simulations.

In contrast to these studies, very little attention has been paid to three-dimensional aspects of the developing region of a wake. Our experience, cited earlier, strongly suggests that some appreciable three-dimensionality should occur in large-scale structures in an otherwise two-dimensional turbulent flow, even in the early stages of evolution of coherent structures; hence the motivation for the present study.

The present experimental work (completed in 1984) was an attempt to examine quantitatively the three-dimensional topology and dynamics of coherent structures in a turbulent shear flow. Here, we persist in our assertion that the spatially phase-correlated vorticity should be the fundamental quantity to characterize coherent structures (Hussain 1980, 1983). Using multiple cross-wire probes, instantaneous distributions of vorticity components in various sectional planes are measured to deduce the spatial configuration of the dominant coherent structures. The detection and eduction techniques to be used have been developed in our previous work (HH; see also Tso 1983; Tso & Hussain 1989). The measurements are made in the intermediate region of a circular cylinder wake; the large-scale spanwise vortices shed from the cylinder are largely in a process of gradual decay, undergoing significant three-dimensional distortion. To our knowledge, this is the first attempt at simultaneous multi-plane vorticity measurements and eduction of organized structures in a turbulent flow. Some of the results discussed in this paper were presented earlier (Hayakawa & Hussain 1986). Throughout this paper we use 'rolls' to denote the dominant, nominally spanwise structures and 'ribs' to denote longitudinal substructures connecting the rolls.

2. Experimental set-up and procedures

The experiment was carried out in an open-return wind tunnel of the Aerodynamics & Turbulence Laboratory of the University of Houston. The facility, originally designed for a large plane-mixing-layer flow, is described in detail by Hussain & Zaman (1982). A 2.7 cm diameter rigid circular cylinder was installed on the centreline of the test section of a 92 cm × 46 cm cross-section, the cylinder being aligned with the longer side. All data were taken at a constant free-stream velocity $U_0 = 7$ ms^{-1}; the Reynolds number based on the cylinder diameter d was $Re_d = 1.3 \times 10^4$. Measurements were made by eight X-wire probes connected to a 16-channel home-built anemometer set, and velocity signals were stored on digital tape and later analysed with a laboratory computer (HP-2100S).

Ideally, all three components of vorticity must be measured in order to clarify the topological features of three-dimensional structures. However, such a demanding approach is far beyond the present measurement technology; in particular, the multipoint measurement of the streamwise vorticity cannot be easily achieved. The present effort was therefore limited to obtaining the spanwise and transverse components of vorticity in either one or two simultaneous sectional planes in the

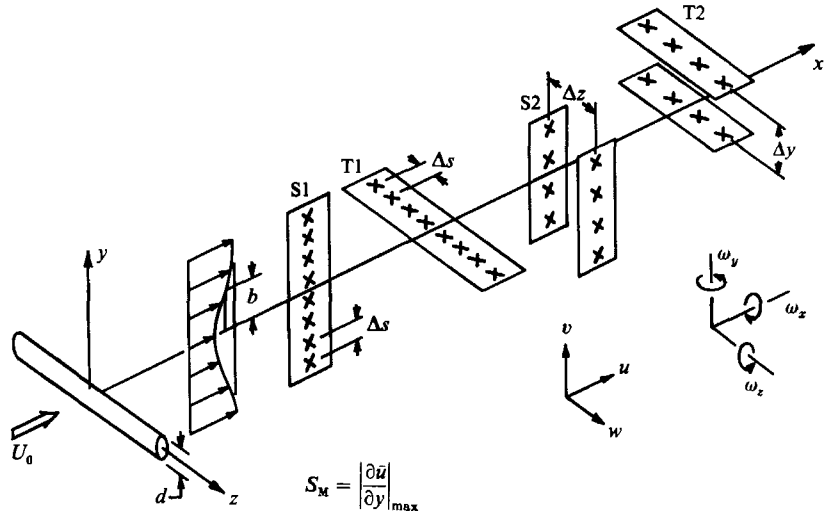

FIGURE 1. Experiment configurations and main notation.

wake. To this end, four configurations of probe arrangements were employed as shown in figure 1; single rakes in configurations S1 and T1, and two parallel rakes in configurations S2 and T2. The rakes S1 and T1 consist of eight equally spaced X-wire probes, and they measure the spanwise and transverse vorticity components respectively. The probe arrangement S2 consists of two parallel rakes separated by a distance Δz in the spanwise direction, each having four X-wire probes, and enables measurements of spanwise vorticities in two parallel (i.e. x, y) planes. Similarly, the probe arrangement T2 measures transverse vorticities in two parallel (i.e. x, z) planes separated by Δy. The distance between the two rakes in the arrangement S2 or T2 can be varied continuously. However, in either arrangement, the two rakes were always positioned in the same streamwise station relative to each other. The crude spatial resolution of the vorticity measurement with either rake, dictated by the laboratory capability, was considered acceptable for the recognition of large-scale events. Figure 1 also shows the coordinate system and some of the relevant flow quantities.

For an array of X-wires in an (x, y)-plane or an (x, z)-plane with a spatial separation Δs between adjacent probes, the vorticity component normal to that plane is, employing the Taylor hypothesis, given by

$$\text{spanwise component:} \qquad \omega_z = \frac{\partial v}{\partial x} - \frac{\partial u}{\partial y} \approx -\frac{1}{U_c}\frac{\Delta v}{\Delta t} - \frac{\Delta u}{\Delta s},$$

$$\text{transverse component:} \qquad \omega_y = \frac{\partial u}{\partial z} - \frac{\partial w}{\partial x} \approx \frac{\Delta u}{\Delta s} + \frac{1}{U_c}\frac{\Delta w}{\Delta t}.$$

Here, Δt denotes the time interval between successive digitized data points, and U_c is the streamwise advection velocity determined experimentally as the celerity of vortical structure centre (see HH). The aggregate sampling rate was 20 kHz (1.25 kHz per channel), giving $\Delta t = 0.8$ ms. Although somewhat crude, we believe that this sampling rate is adequate for the detection of large-scale structures. Instantaneous vorticities are calculated at midpoints between two neighbouring X-wires by the central-difference approximation. Structures are recognized from

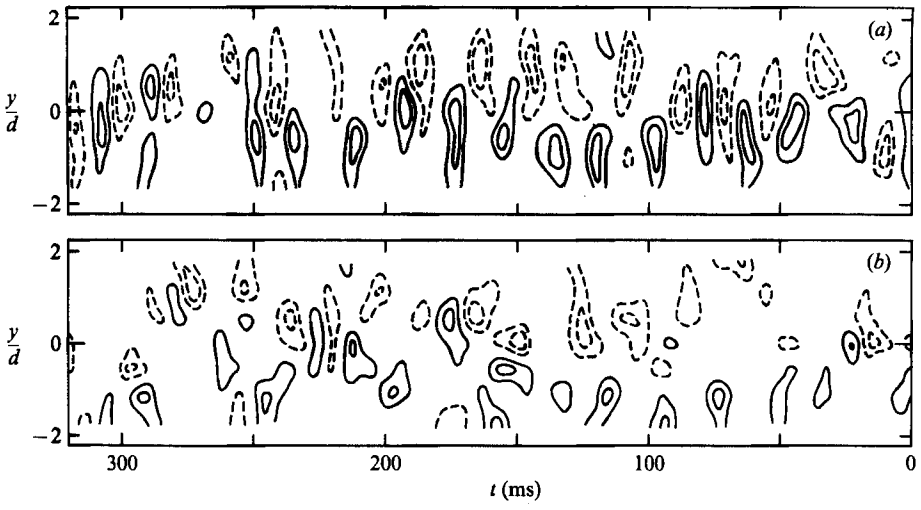

FIGURE 2. Instantaneous $\tilde{\omega}_z$ maps: (*a*) $x/d = 20$, (*b*) $x/d = 40$; contour levels: $\tilde{\omega}_z/S_M = \pm 4, \pm 2$. Time increases from right to left.

appropriately smoothed vorticity signals, the smoothing being done by the short-time averaging technique. Detailed procedures for calculating instantaneous, smoothed vorticity are described by HH. The data presented in this paper are for two streamwise stations: $x/d = 20$ and 40, except for those discussed in §3.

3. Large-scale spanwise structure

3.1. *Instantaneous spanwise vorticity field*

First, in order to illustrate the nature of large-scale structures, two examples of the instantaneous contour maps of (smoothed) spanwise vorticity $\tilde{\omega}_z$ (tilde denotes smoothed quantities) measured by the single rake S1 (with a probe separation $\Delta s = 15$ mm, or $\Delta s/d = 0.56$) at $x/d = 20$ and 40 are shown in figure 2. The figure shows instantaneously occurring temporal events, sliced by the (x, y)-plane, at a fixed streamwise station (for further examples of $\tilde{\omega}_z$ maps, see HH, in which instantaneous $\tilde{u}$- and $\tilde{v}$-maps are also included). Time increases from right to left; this time coordinate, used throughout this paper, implies that the flow is from left to right. Contour levels are normalized by the local maximum time-mean shear rate $S_M = (\partial\bar{u}/\partial y)_{max}$; here, the overbar denotes time-mean quantities. Clockwise and counterclockwise vorticities are denoted by broken and solid lines respectively. If time is transformed into streamwise distance by assuming Taylor's hypothesis (i.e. $x = -U_c t$), the abscissa scale corresponds to about one fourth of the transverse scale. That is, the streamwise coordinate in figure 2 is compressed by a factor of 4 in order to include more structures.

In figure 2(*a*) we can easily identify vortices of alternating circulations passing through a sectional plane ($z = 0$) at $x/d = 20$. Recognizing the relatively short distance from the cylinder, however, it is rather surprising that considerable dispersions in size, strength, transverse displacement and streamwise spacing have appeared, as is particularly evident in the left-hand portion of the figure. The dispersions are much greater at $x/d = 40$ (figure 2*b*). This irregularity of individual structures may be due to various factors such as wandering or deformation of vortices, distortion induced by ribs, spanwise variation in vorticity due to

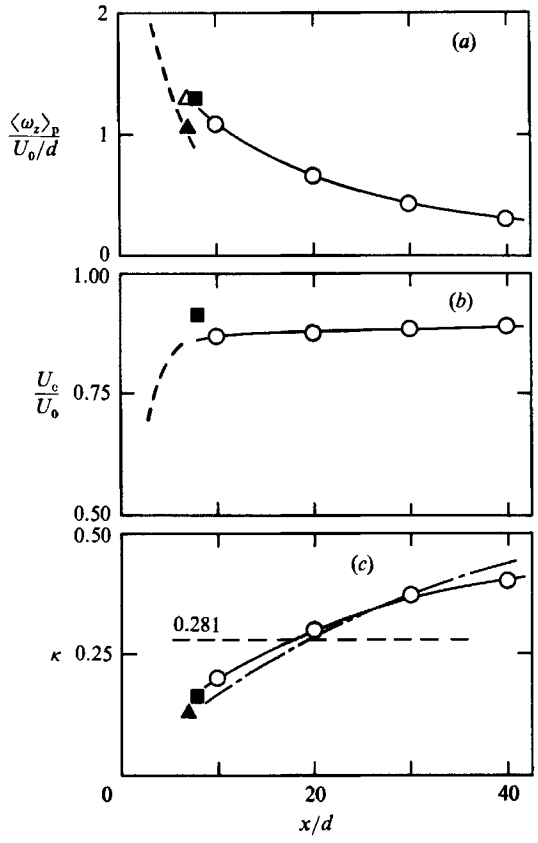

FIGURE 3. Streamwise variation of global properties: (*a*) peak coherent vorticity, (*b*) advection velocity, (*c*) vortex spacing ratio. ○, present data ($Re_d = 1.3 \times 10^4$); ----, Cantwell & Coles (1.4×10^5); ■, Kiya & Matsumura (1.6×10^4); △, ▲, Armstrong *et al.* (2.15×10^4); —·—, Matsui & Okude (80–140).

non-uniform stretching, partial tearing, cut-and-connect (i.e. crosslinking), etc. Regardless of which of these factors is predominant, the spanwise distribution of vorticity becomes non-uniform rapidly in x. Therefore, in order to gain further insight into the wake structure, the three-dimensional aspects of the phenomenon should be investigated.

3.2. *Comparison with other data*

Before proceeding to a consideration of three-dimensional aspects, we show in figure 3 some comparisons of our results from the single rake S1 with recent relevant data from other investigations. This comparison of streamwise variations of global properties characterizing the structure development is included in order to check consistency among data obtained in different laboratories using different facilities and techniques. Figure 3 includes (*a*) ensemble-averaged peak vorticity $\langle\omega_z\rangle_p$, (*b*) structure advection velocity U_c, and (*c*) vortex spacing (i.e. transverse to longitudinal spacing) ratio κ. Among the other studies, Cantwell & Coles (1983) used an upstream triggering method based on the cylinder surface pressure near the separation point, whereas Kiya & Matsumura (1985) and Armstrong, Barnes & Grant (1987) employed local detection schemes. Of the latter two, the first utilized smoothed periodic transverse velocity (v) fluctuations on the wake centreplane and the second used irrotational streamwise velocity (u) fluctuations outside the shear region as the

reference signals for triggering phase-locked measurements. Reynolds number(s) for each experiment are given in the figure caption.

In general, our data are not inconsistent with others' results, and are in fairly good agreement with those of Kiya & Matsumura.† A rather rapid decay of the peak vorticity values obtained by Cantwell & Coles seems primarily due to the jittering effect inherent to their upstream triggering technique. As explained and emphasized by us (e.g. Hussain 1986; HH), such a triggering method can eliminate the initiation jitter but not the trajectory or evolutionary jitter which increases with increasing x. Data of Armstrong *et al.* show a lower $\langle\omega_z\rangle_p$ value in spite of their use of a local detection scheme. This can also be attributed mostly to smearing inherent to their triggering method; their reference probe was located outside the wake region (at $y = 3.2\,d$), thus unavoidably capturing footprints of passing structures whose centres are not expected to bear a unique relationship with the footprint on the trigger signal. In addition, their detection probe was shifted by $0.5\,d$ in the x-direction from the sampling probe, thus further contributing to the smearing. Herein lies what we consider to be the superior feature of our eduction scheme: it does not rely on any external trigger signal, but uses the measurement signal (i.e. vorticity at the structure centre) itself as the trigger signal. Our measurements are thus free from the initiation and evolutionary jitters as well as from the footprint ambiguity. Note that the peak vorticity value in the artificially excited wake studied by Armstrong *et al.*, which is denoted by an open triangle in figure 3(*a*), is closer to ours and Kiya & Matsumura's. This suggests that excitation can considerably reduce the evolutionary jitter of structures.

The structure advection velocity (figure 3*b*) increases rapidly in the very near region, say up to $x/d = 6$, and thereafter shows a more gradual increase. The average vortex spacing ratio (figure 3*c*), which is determined from the ensemble-averaged vorticity field and the advection velocity U_c, also increases with increasing x. Note that the chain-link line in figure 3(*c*) represents the laminar wake data ($Re_d = 80$ to 140) of Matsui & Okude (see Matsui 1982). Particularly noteworthy is the fact that the most probable vortex spacing ratio is not significantly altered by the flow state – laminar or turbulent – and in both cases the ratio crosses the theoretical value of 0.281 for the (stable) Kármán vortex street at around $x/d = 20$. The stability of the Kármán street has been studied theoretically by many; some have taken into account the effect of finite core size on the stability (e.g. Kida 1982; Meiron, Saffman & Schatzman 1984). However, these theories assume doubly infinite vortex rows with back-to-fore symmetry and thus cannot account for the continuous increase of the vortex spacing ratio observed experimentally. It is clear that a more realistic predictive theory must take into consideration the streamwise evolution of the wake, as also pointed out by Jimenez (1987).

3.3. *Importance of the saddle region*

Various structure measures and the associated turbulence characteristics are discussed in HH. Here, we reproduce in figure 4 the contours of coherent strain rate (denoted by bold lines) and production of incoherent turbulence (broken lines) at $x/d = 20$ in order to illustrate the important role of the saddle region in the turbulence production mechanism. In this figure, dotted lines denote the coherent structure boundaries, designated by the coherent vorticity contour level of $\langle\omega_z\rangle/S_M = 1$; the

† HH and Kiya & Matsumura used selective conditional-sampling methods. The number of finally accepted structures is $0.36f_s$(i.e. 36%) at $x/d = 10$ in HH, and $0.43f_s$(i.e. 43%) at $x/d = 8$ in Kiya & Matsumura. Here, f_s is the number of shed vortices on one side of the wake.

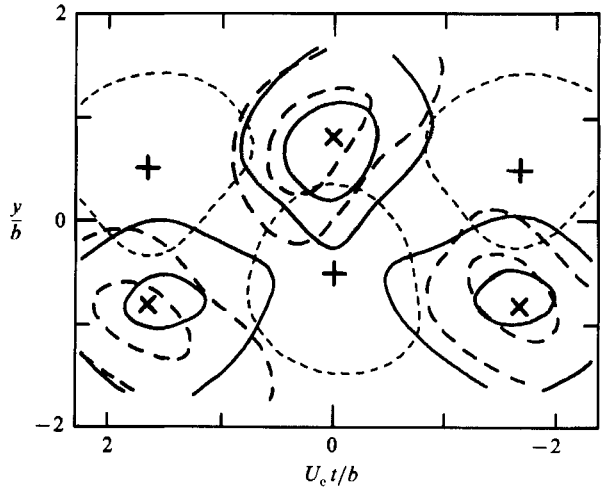

FIGURE 4. Typical structure properties, focusing on the significance of the saddle region (a two-dimensional cut at $x/d = 20$): ----, structure boundary ($\langle\omega_z\rangle/S_M = 1.0$); ——; coherent strain rate ($\langle S\rangle/S_M = 2.0, 1.0$); – – – –, coherent production ($\langle P\rangle/U_0^2 S_M = 0.008, 0.004$).

'centres' and the 'saddles' are marked as + and × respectively. Note that the contour shapes on the upper and lower side of the wake are not exactly the same; this is because the eduction is triggered and aligned with respect to the structure centre at $t = 0\,(y < 0)$ and thus educed flow properties away from the trigger point suffer from unavoidable smearing. Large-scale structures produce the intense strain rate in the saddle region; accordingly, the production of smaller-scale turbulence due to the large-scale structures occurs in this region (Hussain 1980). This can be attributed to the vortex stretching along the braid that connects successive spanwise vortices, as discussed by Cantwell & Coles (1983) and HH. Thus, the braid would not be a continuous two-dimensional sheet, but would consist of three-dimensional 'ribs' characterized by longitudinal vorticity (Hussain 1984). Since streamwise streaky structures or ribs have been observed in the braids in several flow visualization studies of plane mixing layers, we expected that ribs exist in the wake as well. In this connection, we wish to re-emphasize a point made repeatedly by us regarding flow visualization: flow visualization can be grossly misleading and must be checked by quantitative data in unsteady and turbulent flows, where flow markers should be introduced locally, if possible. Flow markers are rapidly depleted from regions of intense vortex stretching and typically accumulated in regions of low vorticity interactions; they thus can distract attention away from regions of dynamical interest.

4. Organization of the spanwise structure

4.1. *Two-rake measurements*

Observations of instantaneous $\tilde{\omega}_z$ maps (figure 2) led us to believe that the spanwise rolls should be subjected to significant distortion. Then, to what extent does an individual roll preserve its spanwise uniformity, and how can we determine quantitatively the extent of spanwise homogeneity, using a limited number of probes? We used two rakes with probe arrangement S2 (figure 1) and measured the spanwise vorticity simultaneously in two (x, y)-planes. Since each rake had only four X-wire probes (giving vorticity values at three midpoints), rather poor resolution was

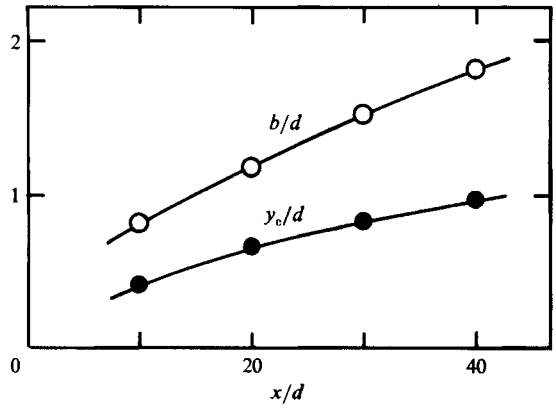

FIGURE 5. Streamwise variation of the wake half-width b and the most probable location y_c of structure centres.

inevitable. To improve the spatial resolution, the central location of each rake was shifted from the wake centreplane so that the rake captured only structures passing on one side of the wake. The transverse distance between adjacent probes was adjusted to 20 mm (or $\Delta s/d = 0.74$) in order to cover the average transverse extent of typical large-scale structures (HH). For reference in the following discussion, the wake half-width b and the average location of structure centre y_c as a function of x are shown in figure 5. Note that the y_c-location is always much closer to the wake centreplane than b; see HH for discussion.

Two examples of simultaneous $\tilde{\omega}_z$ contours are shown in figure 6, for the spanwise separation $\Delta z = 3d$ which corresponds to $2.5b$ at $x/d = 20$ and $1.7b$ at $x/d = 40$ respectively. The transverse location of each rake centre is at $y \approx 0.5b$. For clarity, the figure includes voriticity contours with one sign only. At $x/d = 20$ (figure 6*a*) we find one-to-one correspondence between $\tilde{\omega}_z$ concentrations in the two planes; this indicates that the rolls are generally continuous over a z-range of much more than $3d$. However, the corresponding contours show considerable differences between the two planes in size, strength, and transverse and/or timewise location. Thus, even though they are continuous, individual rolls appear highly distorted, and the ω_z component of such rolls depends on the local inclination to the (x, y)-plane. At $x/d = 40$ (figure 6*b*) the correspondence between the two planes is much weaker than at $x/d = 20$; quite frequently, structures appear in only one of the two planes. This behaviour may result from two causes: (1) continuous rolls escape either rake because of the limited y-range covered by the rake, and (2) 'discontinuous' structures actually occur due to significant tilting and diffusion (see §5.2).

Recalling the fact that these contour plots have been obtained by filtering out high-frequency vorticity fluctuations and by retaining only largescale vorticity fields, there should be little doubt that the wake structure is fairly three-dimensional even at the largest scale.

4.2. *Spatial correlation of spanwise vorticity*

In order to quantify the three-dimensionality, the spanwise correlation $\overline{\tilde{\omega}_z \tilde{\omega}_z(\Delta z)}$ of (smoothed) spanwise vorticities was measured using the same probe arrangements as used for figure 6. Each correlation was calculated between vorticity signals obtained at the same y-location but in two different (x, y) planes. Results are shown in figure 7(*a*); data at two y-locations are included for each of the two x-stations, and the

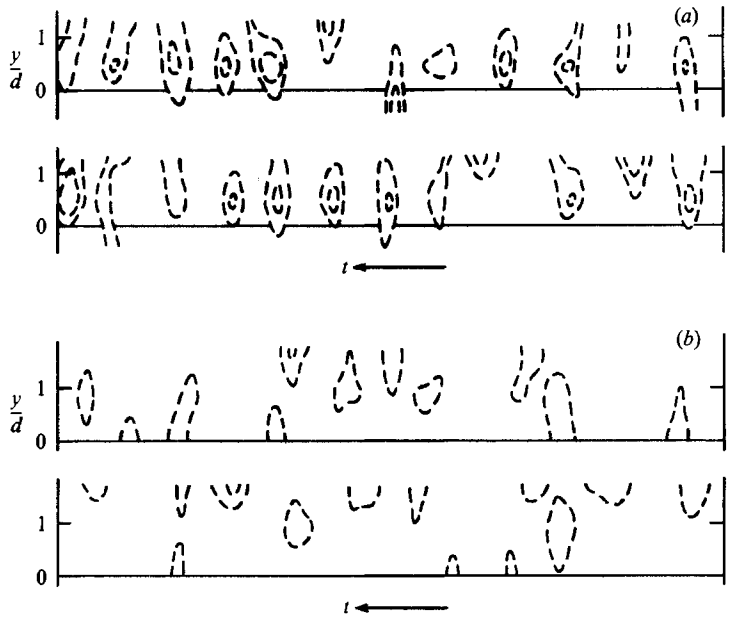

FIGURE 6. Instantaneous $\tilde{\omega}_z$ maps measured simultaneously at two (x, y)-planes ($\Delta z = 3d$); (a) $x/d = 20$, (b) $x/d = 40$; contour levels: $\tilde{\omega}_z/S_M = -4, -2$.

correlation value is normalized by the r.m.s. values of $\tilde{\omega}_z$ and $\tilde{\omega}_z(\Delta z)$. Despite high-frequency (i.e. smaller scale) fluctuations being smoothed out, the correlation coefficient R decreases rapidly with increasing Δz. For both x-stations, the dotted-lined correlation curve obtained at a y-location close to the half-width location b, is lower than the solid curve for $y \approx 0.5b$. This is to be expected because the most probable y-location for the centre of rolls is $y \approx 0.5b$ (see figure 5); thus the (long-time) correlation should be highest along this y-location. The relatively small difference between data for $y \approx b$ and $y \approx 0.5b$ at $x/d = 40$, compared with the difference at $x/d = 20$, can be attributed to increased transverse wandering (i.e. increased broadening of the transverse probability distribution) of structure centres with increasing x (see figure 3 in HH).

In figure 7(b), the data at $y \approx 0.5b$ are replotted using a semilogarithmic scale. The correlation coefficient shows a nearly exponential decay with the spanwise separation for $\Delta z > d$. One can (somewhat arbitrarily) estimate the spanwise scale of structures to be the separation at which the correlation coefficient drops by e^{-1}. The spanwise scales thus determined from figure 7(b) are $\Delta z = 1.8d$(or $1.5b$) at $x/d = 20$ and $\Delta z = 0.9d$ (or $0.5b$) at $x/d = 40$.

4.3. *Ensemble average of spanwise vorticity*

The spanwise organization of the rolls was investigated further by taking the ensemble average of ω_z in planes parallel to (but separated by Δz from) a reference (x, y)-plane. Again, the midpoint of each rake was located at $y \approx 0.5b$.

The detection criteria adopted here for identifying structures at the reference plane were relatively less stringent than those used in HH. Specifically, the steps were: (1) to detect structures that are centred at the mid-point y_c of the rake by requiring $\tilde{\omega}_z(y_c)$ to be transversely maximum, i.e. simultaneously higher than $\tilde{\omega}_z(y_c + \Delta s)$ and $\tilde{\omega}_z(y_c - \Delta s)$; (2) to specify the structure strength and the streamwise

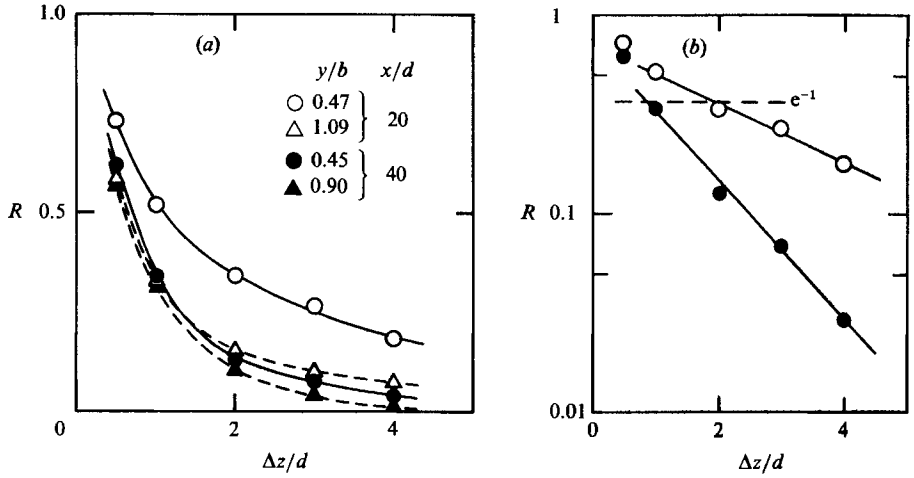

FIGURE 7. Spanwise correlation coefficient R of $\tilde{\omega}_z$; (*a*) linear scale, (*b*) semi-logarithmic scale. $R = \overline{\tilde{\omega}_z \tilde{\omega}_z(\Delta z)}/\{\overline{\tilde{\omega}_z^2}\,\overline{\tilde{\omega}_z^2(\Delta z)}\}^{\frac{1}{2}}$.

structure size by requiring $\tilde{\omega}_z(y_c)$ to be higher than a threshold ω_{th} for time duration ΔT; (3) to determine the timewise (i.e. streamwise) structure centre location t_c as the central time when $\tilde{\omega}_z(y_c)$ is above the threshold (i.e. as the midpoint of the duration ΔT); and (4) to specify the transverse structure size by requiring that $\tilde{\omega}_z(y_c \pm \Delta s, t_c)$ have the same sign as that of the centre (y_c, t_c). After some iterative tests, the threshold value and the duration were selected as $\omega_{th} = 2.5 S_M$ and $\Delta T = 3.2$ ms $= 0.17 T_s (U_c \Delta T \approx 22$ mm); here, T_s is the mean period of vortex shedding on one side of the cylinder.

Following this detection algorithm, we can identify individual structures whose centres are located at (y_c, t_{ci}); t_{ci} is the location in time of the centre of the ith structure. Large-scale structures are accepted only when these criteria are satisfied simultaneously so that weaker, smaller or transversely shifted structures are not included as 'reference structures' (i.e. the structures detected in the reference (x, y)-plane). The iterative alignment of structure centres (followed by HH) is not done in the present analysis because we are not concerned here with detailed incoherent and coherent structure properties. With the reference structure centre as a phase (i.e. time) reference, a signal segment, around t_{ci}, of *unsmoothed* vorticity in a plane separated by Δz from the reference plane is aligned with respect to the corresponding reference structure centre (y_c, t_c), and then ensemble averaged.

The results are shown in figure 8(*a*) for $x/d = 20$ and figure 8(*b*) for $x/d = 40$. The ensemble average was calculated over about 100 and 150 realizations for $x/d = 20$ and 40 respectively. Contour levels are non-dimensionalized by S_M; broken lines denote clockwise vorticity associated with the reference structure and solid lines (clockwise vorticity) show structures shed from the opposite side of the cylinder. In each figure, the lowest contour indicates the reference structure. The peak of the educed vorticity decreases with increasing Δz. Since the reference structure is educed by minimizing spatial jitter and discarding weaker or smaller structures, these data should reflect a substantial lack of two-dimensionality of rolls. The peak value of $\langle \omega_z \rangle$ decreases down to one-half of the reference value at a spanwise separation of $\Delta z = (3\text{–}4)\,d$ at $x/d = 20$ and of $\Delta z = (1\text{–}1.5)d$ at $x/d = 40$; with respect to the local half-width b, these values are roughly $3b$ and $0.7b$ respectively, which are somewhat larger than those determined from the spatial correlation (figure 7). As the detection

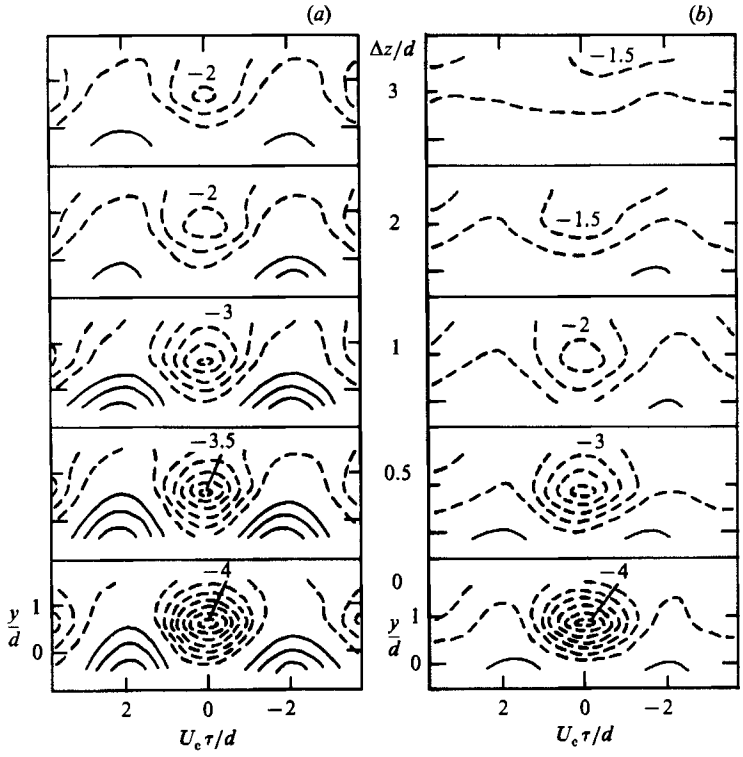

FIGURE 8. Ensemble-averaged $\tilde{\omega}_z$ contours for various spanwise separations: (*a*) $x/d = 20$, (*b*) $x/d = 40$.

scheme has selectively captured 'typical' large-scale structures only, the number of accepted structures was $0.35f_s$ and $0.23f_s$ (i.e. 35% and 23% of initially shed structures) at $x/d = 20$ and 40 respectively. The mean spanwise scale of all rolls, which include relatively smaller or weaker structures discarded in the eduction process, should be actually smaller than that inferred from figure 8. This may be the reason why the spanwise scale obtained by the spatial correlation is smaller than that obtained from the ensemble averaging.

4.4. *Spanwise scale of rolls*

Summarizing the results of spanwise vorticity correlations and conditional-averaging analyses, we conclude that the typical spanwise scale of the primary vortices is indeed quite small. We recall that by intentionally imposing a spanwise variation in the trailing edge of a splitter plate, Breidenthal (1980) observed that the wake had much longer 'memory' of the spanwise perturbation (than a mixing layer), even though the side view, i.e. (x, y)-plane (of this three-dimensional flow) appeared quite similar to that of a two-dimensional wake. Thus, any measurement or visualization simply done in particular (x, y)-planes could overlook the real three-dimensional structure even in the near wake.

Unfortunately, little attention has been paid to the spanwise scale of the large-scale structures in the cylinder wake. Here, we briefly compare our results with those reported by Browand & Troutt (1985), who measured the spanwise correlation of longitudinal velocity fluctuations of two-stream mixing layers with the aid of a rake of 12 single hot-wires and estimated the spanwise scale as a function of the speed

ratio $\Delta U/\bar{U}$(ΔU and $\bar{U}$ are difference and average of the two stream velocities). The extrapolation of their data to the wake case (i.e. the speed ratio of zero) results in an asymptotic spanwise scale – defined by a 40% correlation point – somewhat larger than $4\delta_\omega$, δ_ω being the local vorticity thickness (see their figure 9). For our data, the corresponding vorticity thickness (evaluated by $\delta_\omega = U_1/(\partial\bar{u}/\partial y)_{\max}$, where U_1 is the mean velocity defect on the wake centreplane) is $1.95d$ at $x/d = 20$ and $3.1d$ at $x/d = 40$. The spanwise extent of rolls determined by the correlation (figure 7*b*) is roughly $0.95\delta_\omega$ and $0.3\delta_\omega$ for $x/d = 20$ and 40 respectively. These values are significantly smaller than those corresponding to the self-preserving region of a flat-plate wake. Although a direct comparison of the present result with the one extrapolated from Browand & Troutt's data in mixing layers is not very rigorous, there is no reason to believe that structures in the far-field wake of a flat plate are much more two-dimensional than those in the intermediate region of a cylinder wake. Contrary to the observations of Browand & Troutt and others (e.g. Wygnanski *et al.* 1979), a three-dimensional direct numerical simulation (Metcalfe *et al.* 1987*a*) shows that the spanwise rolls in a fully turbulent mixing layer are intensely three-dimensional (see also Hussain 1986). Moreover, Browand & Troutt's data show an increase in the spanwise coherence with decreasing speed ratio; this trend appears counter to the fact that the mixing layer is relatively more stable to three-dimensional disturbances than the wake (Breidenthal 1980; Robinson & Saffman 1982).

Note that observations based on the velocity fluctuations induced by organized structures are very likely to capture not the 'substance' but the 'shadow' of the underlying structures. We suggest therefore that the apparent discrepancies mentioned above should be resolved through quantitative studies based on coherent vorticity measurements.

5. Transverse vorticity concentrations

5.1. *Instantaneous transverse vorticity field*

As a next step in exploring the three-dimensional nature of the wake, the transverse vorticity component ω_y was measured by using the rake T1. The rake was placed on one side (i.e. $y > 0$) of the wake. The distance between adjacent probes was 15 mm (i.e. $\Delta s/d = 0.56$), the total distance spanned by the rake being about $4d$. This probe spacing was chosen as a compromise between the requirements of covering a larger region of the flow and having acceptable spatial resolution.

Some examples of (smoothed) instantaneous $\tilde{\omega}_y$ maps are shown in figures 9 and 10 for $x/d = 20$ and 40. Each figure includes two maps measured at different transverse locations (i.e. (x, z)-plane); one is close to the half-width location ($y = b$) and the other is near the average location of primary spanwise structure centres ($y \approx 0.5b$). Contour levels are again non-dimensionalized by S_M so that the strength of $\tilde{\omega}_y$ concentrations can be directly compared with those of $\tilde{\omega}_z$ shown in figure 2. Clockwise (negative) and counterclockwise (positive) vorticity levels are denoted by broken and solid lines respectively. Note that the contour levels drawn are higher for $x/d = 40$ than for $x/d = 20$, while the absolute values are lower at $x/d = 40$ because S_M there is about half of that at $x/d = 20$. The signs of circulations and the mean period T_s of vortex shedding are indicated in the upper portion of figure 9(*a*). The abscissa scale corresponds to about one quarter of the ordinate (i.e. spanwise) scale, as in figure 2.

It is readily seen from these figures that there are large numbers of $\tilde{\omega}_y$ concentrations which are indicative of three-dimensionality of the coherent

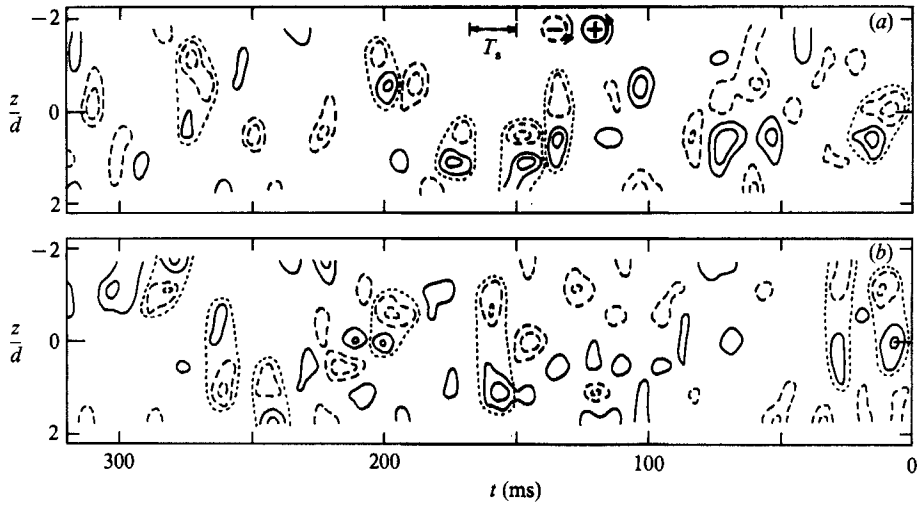

FIGURE 9. Instantaneous $\tilde{\omega}_y$ maps at $x/d = 20$; (*a*) $y/b = 0.94$, (*b*) $y/b = 0.47$; contour levels: $\tilde{\omega}_y/S_M = \pm 3, \pm 1.5$. Dotted lines indicate paired $\tilde{\omega}_y$ concentrations with opposite circulations. The direction of circulation and the mean vortex shedding period are depicted in the upper portion of figure (*a*).

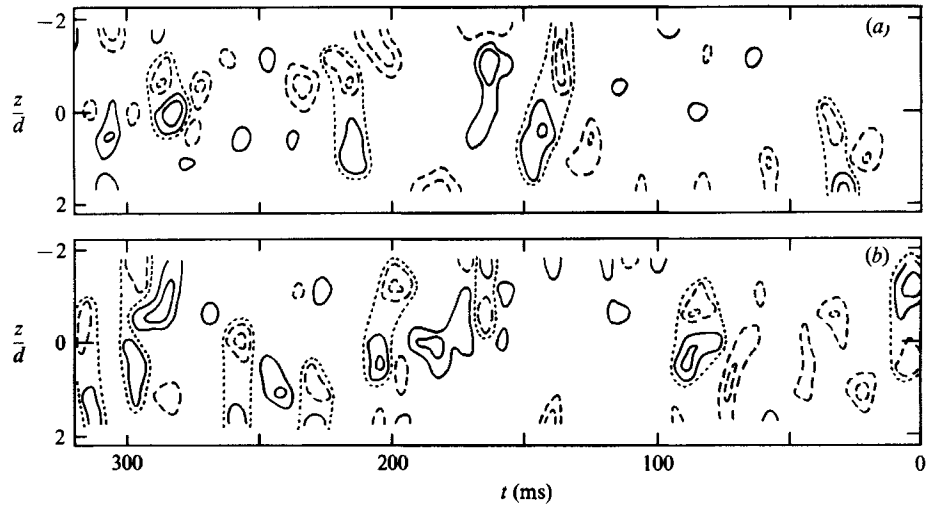

FIGURE 10. Instantaneous $\tilde{\omega}_y$ maps at $x/d = 40$; (*a*) $y/b = 0.82$, (*b*) $y/b = 0.41$; contour levels: $\tilde{\omega}_y/S_M = \pm 4, \pm 2$. For dotted lines and the direction of circulation, see figure 9.

structures. Furthermore, many $\tilde{\omega}_y$ concentrations have strengths comparable with those of $\tilde{\omega}_z$ concentrations (see figure 2). Such strong concentrations of transverse vorticity have not been recognized before. Superficially, the distribution of $\tilde{\omega}_y$ patches appears quite irregular, and it seems difficult to find any specific spatial configuration. However, a closer inspection reveals that $\tilde{\omega}_y$ concentrations tend to have paired patterns with opposite-signed circulations, indicative of counter-rotating vortex pairs. Such patterns are seen in areas enclosed by dotted lines in figures 9 and 10. This feature is not surprising if we consider the kinking or warping of rolls, because the deformation of a spanwise vortex tube (or filament) into a horseshoe or hairpin vortex is an obvious consequence of shear and is indeed a common feature in any plane shear flow (e.g. Pierrehumbert & Widnall 1982).

Three-dimensional instability may be expected to produce periodic spanwise undulations of rolls. However, no clear evidence of spanwise periodicity – which should appear as positive and negative vorticity concentrations aligned periodically in the z-direction – is apparent in the $\tilde{\omega}_y$ maps. Furthermore, we cannot see any clear periodic appearance of $\tilde{\omega}_y$ concentrations in time (i.e. streamwise direction) either. Note that these arguments implicitly assume a global two-dimensionality of rolls; that is, undulating or not, they are presumed to remain aligned in the z-direction. However, because the actual flow field is intensely three-dimensional (as inferred from $\tilde{\omega}_y$ maps themselves and also from the results discussed in the previous sections), there is no reason for the $\tilde{\omega}_y$ concentrations to be observed at the same time. Rather, it is more probable that the rolls are considerably distorted not only in the spanwise direction but also in the streamwise direction. Keeping this in mind, we can recognise some occasions (within short time segments) when $\tilde{\omega}_y$ contours change their signs alternately in the z-direction: for examples, at $t \approx 70$ ms in figure 9(a), at $t \approx 120$, 210 and 225 ms in figure 9(b), at $t \approx 280$ ms in figure 10(a), and at $t \approx 200$ ms in figure 10(b). However, these events are relatively infrequent. In addition, we cannot easily identify whether $\tilde{\omega}_y$ concentrations are manifestations of intrinsic three-dimensionality of rolls or occurrence of ribs (discussed in §6.1).

The irregular instantaneous vorticity maps pose significant difficulties in clarifying detailed topological features of structures from relatively sparse quantitative data. But far more limiting, in our view, are the conventional visualization studies.

5.2. *Ensemble-averaged transverse vorticity*

Next, using the instantaneous $\tilde{\omega}_y$ maps, we tried to educe a plane cut of transverse structures. That is, by identifying the $\tilde{\omega}_y$ peaks of a specified sign, we aligned the associated realizations with respect to those peaks and obtained ensemble averages of ω_y. Essentially the same procedure used in the previous section for ω_z data was followed. The detection criterion was to specify the structure strength and streamwise size by requiring that $\tilde{\omega}_y$ at the rake centre be higher than a given threshold ω_{th} for a certain duration (in this case, 3.7 ms or $0.2T_{\text{s}}$). This streamwise scale is roughly equal to half of the typical roll size determined in HH. After examining the instantaneous maps, the threshold level ω_{th} was chosen as $2S_{\text{M}}$ and $2.6S_{\text{M}}$ for $x/d = 20$ and 40 respectively.

Ensemble averages of ω_y thus obtained over more than 200 realizations are shown in figures 11(a–c) and 12 (a–c). Figures (a, b) are obtained from the detection of positive $\tilde{\omega}_y$ concentrations, and the figure (c) from the detection of negative $\tilde{\omega}_y$ concentrations. Each figure indicates opposite-signed vorticity concentrations located preferentially at one side of the detected structure in such a manner that a larger negative $\langle\omega_y\rangle$ contour appears in the negative z-range when triggered by the positive $\tilde{\omega}_y$, (a and b), and vice versa when triggered by the negative $\tilde{\omega}_y$, (c).

The accepted number of $\tilde{\omega}_y$ concentrations is $(0.17\text{–}0.22)f_{\text{s}}$ at $x/d = 20$ and $(0.13\text{–}0.17)f_{\text{s}}$ at $x/d = 40$ (the number decreases slightly with increasing y within the y-range covered here), while the strength of the $\tilde{\omega}_y$ concentration is larger at $x/d = 40$. Considering that the threshold level used was relatively higher at $x/d = 40$, it may be said that the number of 'typical' (i.e. accepted) transverse structures is not significantly different between the two x-stations. Recall that the number of rolls detected at the most probable y-location of their centres decreases from $0.35f_{\text{s}}$ at $x/d = 20$ to $0.23f_{\text{s}}$ at $x/d = 40$ (see §4.3; the number decreases by a factor of two in HH, where stricter criteria were used for eduction). One can conclude from the above observation that the decrease in size of 'typical' rolls with increasing x is not

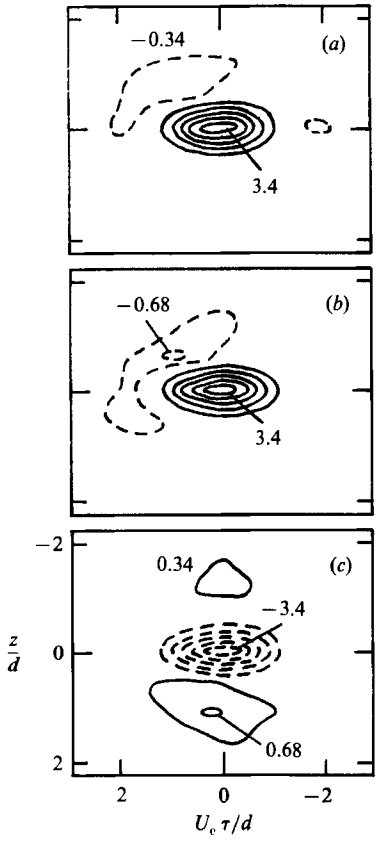

FIGURE 11.

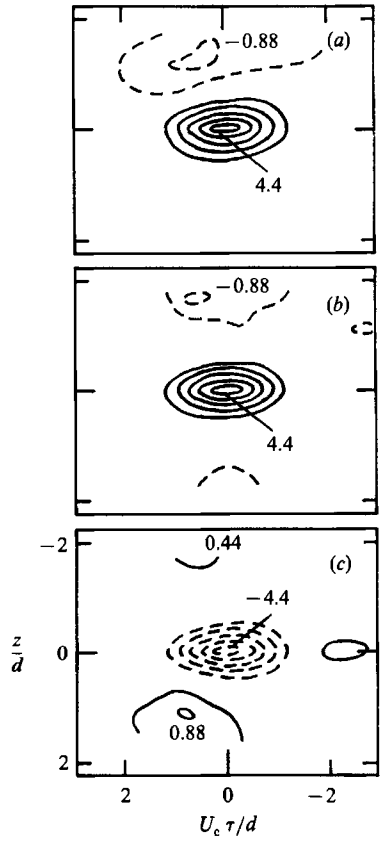

FIGURE 12.

FIGURE 11. Ensemble-averaged $\tilde{\omega}_y$ contours at $x/d = 20$; (*a*) $y/b = 0.94$, (*b*) $y/b = 0.47$, (*c*) $y/b = 0.47$. Note that stronger non-reference structure appears preferentially on one side of the reference structure.

FIGURE 12. Ensemble-averaged $\tilde{\omega}_y$ contours at $x/d = 40$; (*a*) $y/b = 1.22$, (*b*) $y/b = 0.82$, (*c*) $y/b = 0.82$. Note that $\langle\tilde{\omega}_y\rangle$ patterns are essentially the same as in figure 11.

due so much to their breakdown into smaller structures but more to their three-dimensional deformations, including spanwise variation of their cross-section.

Once again, there is no clear indication, in figures 11 and 12, of spanwise periodicity of transverse structures; if there were, opposite-signed vorticities should be educed on both sides of the reference structure with equal probability. The direction of circulation suggests that the formation of a transverse vortex pair (i.e. two legs of the same structure) might be initiated more frequently by outward kinking (see figure 13*a*). If the inward kinking (figure 13*b*) is predominant, the positive $\langle\omega_y\rangle$ contour should appear preferentially in the upper side (with respect to the negative $\langle\omega_y\rangle$ contour) in figures 11 (*a*, *b*) and 12 (*a*, *b*). The educed pattern shows just the opposite, indicating the outward kinking occurs more frequently. Note that in the instantaneous $\tilde{\omega}_y$ maps (figures 9 and 10), the most clearly identifiable pairs of $\tilde{\omega}_y$ (denoted by dotted-line envelops) correspond to figure 13(*a*).

In figures 11 and 12, the much weaker contour levels of the educed (non-reference) structure (away from $z = 0$) suggest that vortex pairs do not occur with high probability. However, assuming that a pair denotes the two legs of a horseshoe-type

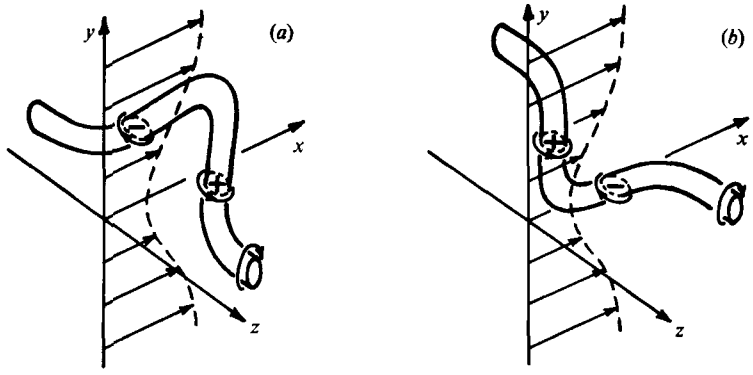

FIGURE 13. Conceptual pictures of deformation of rolls; (*a*) outward kinking, (*b*) inward kinking. Signs (+ and −) indicate those of the $\tilde{\omega}_y$-component.

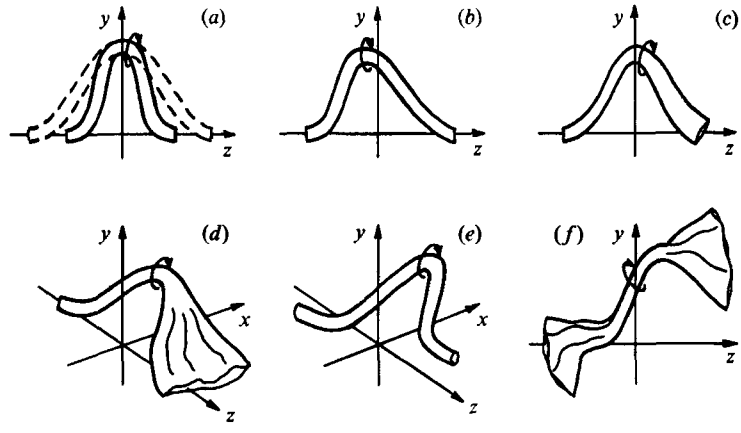

FIGURE 14. Conceptual illustrations of possible configurations of distorted horseshoe-like vortices; (*a*) unequal spanwise spacing, (*b*) asymmetry in the *z*-direction, (*c*) unequal strength, (*d*) diffusion of one leg, (*e*) relative shift in the *x*-direction, (*f*) significant diffusion.

vortex, the relative jitter between the two legs can dilute the ensemble-averaged vorticity level. There are three possibilities: the two legs (1) have equal strength but are asymmetric or have large variations in spanwise spacing even if symmetric; (2) have unequal strength; or (3) are relatively shifted in time. These scenarios are illustrated in figure 14 (*b–e*). We feel that all of them occur frequently in a turbulent environment and the occurrence of horseshoe-like vortices with symmetric legs is not likely to be frequent. Thus, a lack of symmetry – for example, one leg being considerably more flared out and distorted than the other leg (destroying symmetry both in geometry and in vorticity level) – should not be surprising and may indeed be prevalent. This seems to be a primary reason that $\tilde{\omega}_y$ concentrations do not always occur as a clear pair in the instantaneous maps (figures 9 and 10). One must not forget that the schematic of a hairpin vortex in a turbulent flow, though often drawn symmetrically, represents merely a simplified, conceptual picture. Worse yet, the legs of a hairpin-like vortex in a turbulent flow may be so diffuse (say, figure 14*f*) that they may escape detection in probe measurement and flow visualization. In fact, isolated vortices have been observed in direct numerical simulations of wall bounded and homogeneous shear flows (Moin & Kim 1985; Rogers & Moin 1987).

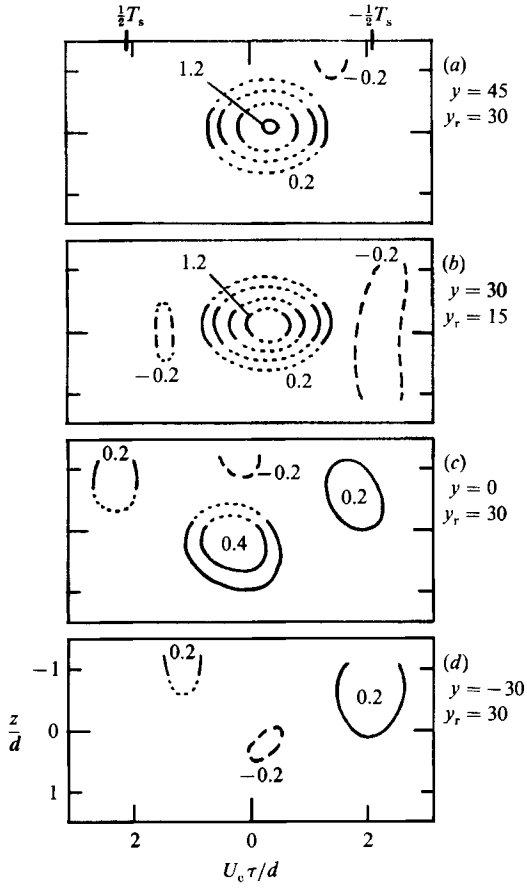

FIGURE 15. Ensemble averages of ω_y at $x/d = 20$ for various combinations of two rakes (the rake arrangement T2).

5.3. *Transverse organization of structures*

Is there any evidence that transverse structures occur in the intermediate wake? For this purpose, using two transversely separated rakes (probe arrangement T2), we detected $\tilde{\omega}_y$ concentrations in a reference plane and obtained the ensemble average of ω_y simultaneously measured in the other plane. The reference rake was placed in one half ($y > 0$) of the wake, while the other rake was positioned sometimes on the same side as the reference rake and sometimes on the other side. For these experiments, the distance between adjacent probes in either rake was 25 mm (or $\Delta s/d = 0.93$); a rather large spanwise separation was used so that transverse structures inclined even in the (y, z)-plane could be captured simultaneously by the two rakes. The detection was based only on positive vorticity concentrations at the midpoint of the reference rake. The eduction procedure is essentially the same as used for the $\langle\omega_z\rangle$ measurement, by the probe arrangement S2 (see §4.3). That is, when the $\tilde{\omega}_y$ in the reference plane exceeds a threshold level ω_{th}, the $\tilde{\omega}_y$ signal in the other plane is aligned with respect to the corresponding reference structure centre and ensemble averaged. The threshold level here is $1.7S_M$ and $2.1S_M$ for $x/d = 20$ and 40 respectively.

Figures 15 (*a–d*) and 16 (*a–d*) show examples of ensemble averages of ω_y at $x/d = 20$ and 40, for various y-locations and distances between the two rakes; the

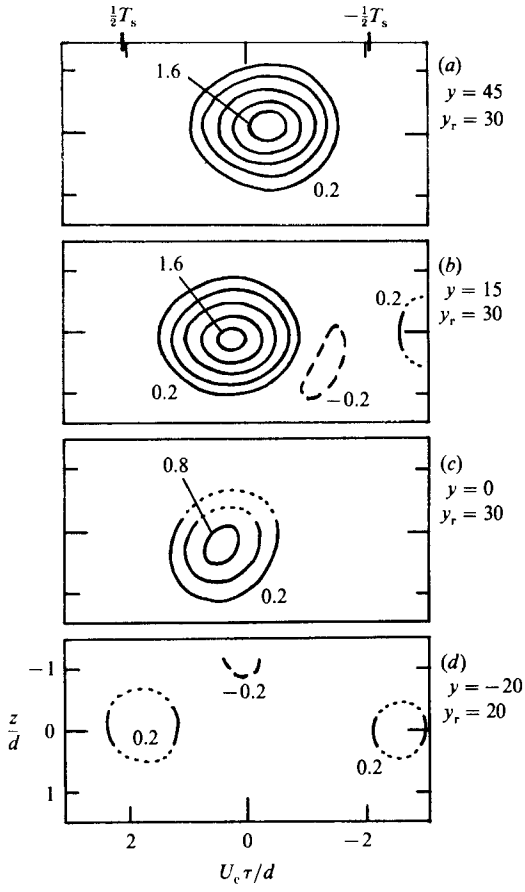

FIGURE 16. Ensemble averages of ω_y at $x/d = 40$ for various combinations of two rakes (the rake arrangement T2).

number of realizations is about 100. The reference rake position is denoted by y_r and the other rake position by y. Again, clockwise (negative) and counterclockwise (positive) vorticities are denoted by broken and solid lines respectively. Note that dotted lines are used wherever clear $\langle\omega_y\rangle$-contours were not apparent owing to sparse data points. At either x-station, closed (positive) contours associated with the $\tilde{\omega}_y$ concentrations at y_r are obtained when both rakes are placed within the transverse range of $y \geqslant 0$. In these cases, the $\langle\omega_y\rangle$-peak is located in $\tau < 0$ and slightly displaced to the negative z-range when $y > y_r$ (i.e. figures 15*a*, *b* and 16*a*), and is located in $\tau > 0$ and $z > 0$ when $y < y_r$ (i.e. figures 15*c* and 16*b*, *c*). Note that no clear coherence is observed when $y_r > 0$ and $y < 0$ (figures 15*d* and 16*d*). This implies that column-like transverse structures extending across the wake centre-plane, similar to the Grant model for the far wake, do not occur in the intermediate region of the wake (for further discussion, see §6.3).

In figures 15 (*c*, *d*) and 16 (*d*), there exist other positive contours located at around $U_c\tau/d = \pm 2$; they are not connected with the structure at y_r. Since this timewise position corresponds nearly to $0.5T_s$ (as denoted at the top of figures 15*a* and 16*a*), these positive contours may indicate transverse structures in the lower side of the wake. At $x/d = 20$ (figure 15*c*, *d*), these $\langle\omega_y\rangle$ contours are displaced in the z-direction away from the educed structure (centred at $z = 0$ and $\tau = 0$). For this situation to

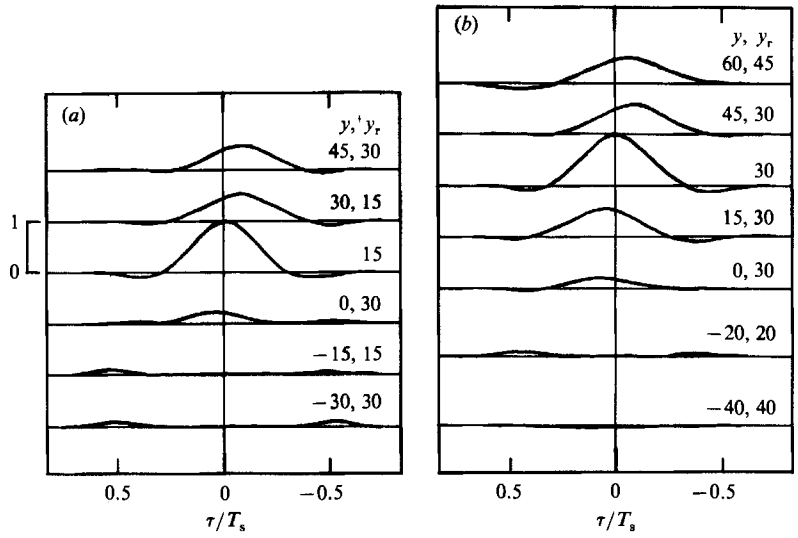

FIGURE 17. Timewise traces of $\langle\tilde{\omega}_y\rangle$ at $z = 0$; (*a*) $x/d = 20$, (*b*) $x/d = 40$. The values are normalized by the peak value at the corresponding y_r.

occur, a probable arrangement of the coherent structures is that of contorted rolls on two sides of the wake being staggered in the z-direction. On the other hand, contours around $\tau = \pm 0.5T_s$ at $x/d = 40$ (figure 16*d*) are located at $z \approx 0$, suggesting that contorted rolls on the two sides are symmetrically aligned in z. Thus, it appears that both configurations, staggered and aligned, would be occurring in the wake, as suggested by HH (see figure 11*d*, *e* of HH). Because of the limited data, however, it is hard to conclude which configuration is more typical, or whether the dominant configuration depends on x-station.

As mentioned earlier, the $\langle\omega_y\rangle$-peak of the educed structure in $y \geqslant 0$ is always located away from $\tau = 0$ and is slightly displaced from $z = 0$. This suggests that the transverse structures are inclined to both the (y, z)-plane and (x, y)-plane. Since the inclination in the (y, z)-plane was small and could not be evaluated owing to sparse data points in z, we tried to determine the inclination in the (x, y)-plane only. Figure 17 (*a*, *b*) shows $\langle\omega_y\rangle$ variations as a function of time on the midlocation of each rake; at this location the $\langle\omega_y\rangle$ value is always the highest of the values at the three discrete z-positions. The $\langle\omega_y\rangle$ values are normalized by the peak value at the corresponding y_r (i.e. $\langle\omega_y\rangle$ at $z = 0$ and $\tau = 0$) because $\langle\omega_y\rangle$ depends somewhat on its transverse location, though the same threshold level is used for all y_r at the same x. The traces at the reference plane are shown only for $y_r = 15$ mm at $x/d = 20$ and $y_r = 30$ mm at $x/d = 40$.

We notice from figure 17 that the transverse structure is inclined to the x-coordinate at an acute angle, in the direction of the mean shear. Small bumps located around $\tau = \pm 0.5T_s$ in $y < 0$ reflect the contorted rolls shed from the lower side of the cylinder, as discussed earlier.

In order to evaluate the inclination angle of the transverse structure in $y \geqslant 0$, we determined the time difference between the peaks of each pair (y, y_r), and successively added the individual time differences to get the total time shift from a fixed y-location (i.e. $y = 30$ mm). Results are shown in figure 18, with the time shift τ multiplied by U_c. Data from the two x-stations collapse roughly onto a single curve. If Taylor's hypothesis (based on a constant advection velocity U_c) is adopted, the

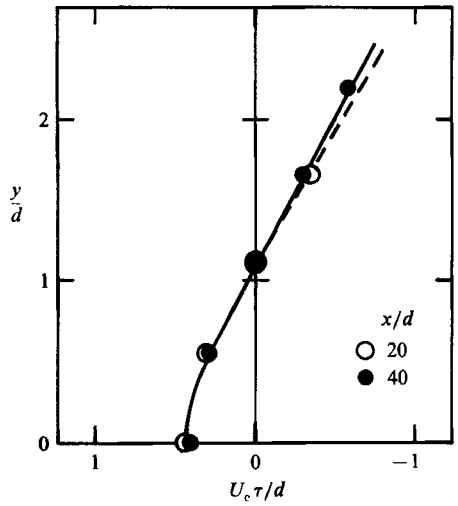

FIGURE 18. Inclination of transverse structures. Time shift τ is obtained with respect to a fixed y-location, i.e. $y = 30$ mm (or $y/d = 1.11$).

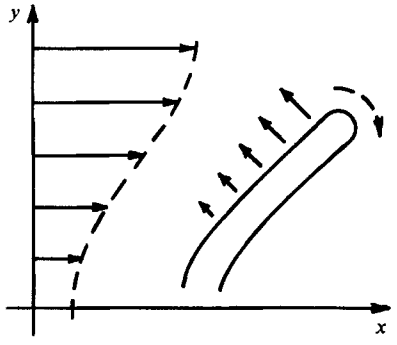

FIGURE 19. Sketch showing a possible mechanism for horseshoe-like vortices to maintain an angle of inclination.

oblique angle from the y-axis is about 30°, except in the vicinity of the wake centreplane. This result suggests that the typical transverse structure has a nearly constant inclination angle irrespective of x-station. How then can structures maintain a constant angle under the persistent effect of the mean strain? A possible explanation may be that while a horseshoe-like vortex tends to be pulled down by the mean strain, the naturally induced velocities of paired legs make the vortex stand up (see figure 19). Since the distance between the two legs decreases as the 'tip' of the horseshoe vortex is approached, the induced velocity is relatively larger in the outer region, as shown by bold arrows in figure 19. Thus the horseshoe-like vortex might maintain a nearly fixed angle owing to two opposing effects: the self-induction of the vortex and the tilting due to the mean strain. Note that contrary to the case of inclined hairpin vortices in the boundary layer (Head & Bandyopadhyay 1981), the mean strain decreases near the 'feet' of the vortex in the wake. This might explain the smaller inclination angle near the centreplane in figure 18.

One may question the use of U_c to infer the spatial orientation of a transverse structure. If the local mean velocity is used instead, the inclination angle increases slightly (as shown by a broken line in figure 18); yet the angle is still much less than

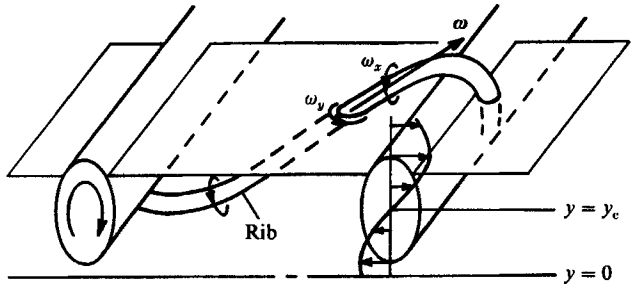

FIGURE 20. Illustration of the detection of ribs using $\tilde{u}$- and $\tilde{\omega}_y$-signals. For simplicity, rolls are drawn as a two-dimensional event.

45°, which is the principal axis of the mean strain-rate tensor. For the far-field structures, the angle of 45° has been frequently mentioned as a typical inclination angle of the roller eddies (e.g. Savill 1983; Mumford 1983) without any definite quantitative basis, while LaRue & Libby (1974) and Bonnet, Delville & Garem (1986) obtained an inclination angle of organized motion with respect to the y-axis of about 30°, in apparent agreement with our observations. Thus, it seems possible to conclude that the most probable inclination angle of the transverse structure in the wake is about 30°. However, since the earlier measurements used the cross-covariance of velocity, intermittency or temperature signals, it is not clear whether those results convey directly the features of large-scale transverse structures. Note also that the present result itself has been based on vorticity measurements in essentially only two (x, z)-planes. Thus, in order to resolve this question of the inclination angle, it would be necessary to use a more sophisticated experimental technique or (perhaps) three-dimensional numerical simulation.

6. Further considerations

6.1. *Longitudinal substructures: ribs*

The present data show that the two-dimensionality of shed vortices disappears much sooner than our intuitive impression suggests. One of the factors producing three-dimensionality seems to be the formation of 'ribs', as mentioned in §1. Since the ribs are characterized primarily by streamwise vorticity, the present measurement cannot capture such longitudinal structures directly. However, because the ribs, being inclined in the (x, y)-plane would intersect the (x, z)-plane between successive rolls, their signatures should appear in this plane as instantaneous $\tilde{\omega}_y$ concentrations. A conceptual sketch showing two rolls and a rib connecting them is shown in figure 20. Note that, for simplicity, the figure includes only one side of the wake, and the rolls are drawn as two-dimensional structures. Based on this viewpoint we tried to search for rib signatures. A question then arose as to how to discriminate $\tilde{\omega}_y$ concentrations due to ribs from those due to distorted rolls, and how to recognize the two different coherent structures without having to simultaneously measure spanwise and normal vorticities.

Let us examine the velocity field associated with the passage of a roll. As a vortex roll passes, the instantaneous streamwise velocity $u(y)$ outside the vortex centre $y_c(y > y_c)$ must be higher than the vortex celerity U_c. According to HH the maximum of the ensemble-averaged u-component at $x/d = 20$ is about $1.3U_c$ at $y = 1.9y_c$, which is roughly the average location of the outer edge of the core of a roll. On the other

hand, the ω_y-component of ribs is likely to be largest at the (x, z)-plane passing through the axes of successive rolls, i.e. at $y = y_c$. Therefore, by putting the rake T1 between these two particular y-locations (i.e. at $y_c < y < 1.9y_c$; see figure 20), one can expect to find some signature of ribs in the instantaneous $\tilde{\omega}_y$-maps by simultaneously examining the corresponding $\tilde{u}$-maps.

Figure 21 (*a–f*) shows three sets of simultaneous records of $\tilde{\omega}_y$ and $\tilde{u}$ at $x/d = 20$. Data are taken at $y = 0.94b$ (or $1.65y_c$), which location satisfies the requirement specified above. The spanwise extent covered by the rake is $3.4b$. In each pair of plots, the upper trace (a, c, e) is $\tilde{\omega}_y$ and the lower (b, d, f) is the corresponding $\tilde{u}$. Contour levels of the latter are given by the deviation from U_c in the non-dimensional form $(\tilde{u} - U_c)/U_0$; positive and negative contours are denoted by solid and broken lines respectively. The abscissa scale in these figures corresponds to about one third of the ordinate (spanwise) scale.

Comparing $\tilde{\omega}_y$- and $\tilde{u}$-maps, when $\tilde{u}$-contours are elongated in the z-direction (beyond the 3:1 aspect ratio because of time compression in the figures), hardly any significant transverse vorticity is observed; at these instants, the (locally) two-dimensional rolls presumably advect under the rake. Such cases are seen at $t \approx 45$, 130, 155 and 175 ms in figure 21 (*a*, *b*), at $t \approx 10$, 120, 170 and 210 ms in figure 21 (*c*, *d*), and at $t \approx 95$, 115 and 170 ms in figure 21 (*e*, *f*). Considering these footprints, the timewise locations of rolls can be roughly estimated by assuming a constant duration between consecutive rolls, equal to the mean period T_s of vortex shedding. The qualitatively inferred locations are denoted by vertical arrows on the tops of $\tilde{u}$-maps.

When there are paired $\tilde{\omega}_y$-concentrations with opposite circulations located near the arrow-marked positions (area surrounded by dotted lines), lower-speed velocity contours (dot-filled contours) appear in the regions between those $\tilde{\omega}_y$ pairs. This is consistent with the fact that paired transverse structures (legs of horseshoe-like vortices) transport lower-momentum fluid from the inner wake toward the outer region, or the vortex induces a velocity in the upstream direction, i.e. opposite to the main flow. We believe therefore that this behaviour results directly from the rolls distorted in such a form as in figure 13 (*a*).

On the other hand, if $\tilde{\omega}_y$-concentrations occur at phases between consecutive $\tilde{u}$-contours which are elongated in the z-direction, they might be regarded as ribs. Now, examining figure 21 (*a*, *c*, *e*), we can see several $\tilde{\omega}_y$-concentrations (hatched contours) located between the elongated $\tilde{u}$-contours or located near the distorted rolls (enclosed by dotted lines). Thus, it seems plausible that these hatched contours indicate the presence of ribs. Note that some of them also have a counter-rotating paired pattern.

Caution must be made here, however, that many of the hatched contours are located near the middle of the successive arrows or even closer to the downstream side of the elongated $\tilde{u}$-contours. This feature would appear to be counter to our initial working assumption, in that the rib signatures should be observed mostly in the region near the upstream side of the elongated $\tilde{u}$-contours. A possible explanation for this is that the $\tilde{\omega}_y$-concentrations located immediately downstream of a roll depict the parts of ribs wrapping around a roll and intruding into its downstream side at which the $\tilde{\omega}_y$-component of ribs can be larger than that in the middle between the successive rolls (see figure 20). However, this is no more than speculation because a three-dimensional numerical simulation by Metcalfe *et al.* (1987*b*) shows that the ribs in a mixing layer need not occur as clear pairs nor completely bridge over consecutive rolls. This is not surprising because vorticity in the braid region is not necessarily totally aligned with the diverging separatrices; as the rolls are approached, vortex lines would flare out to wrap around rolls.

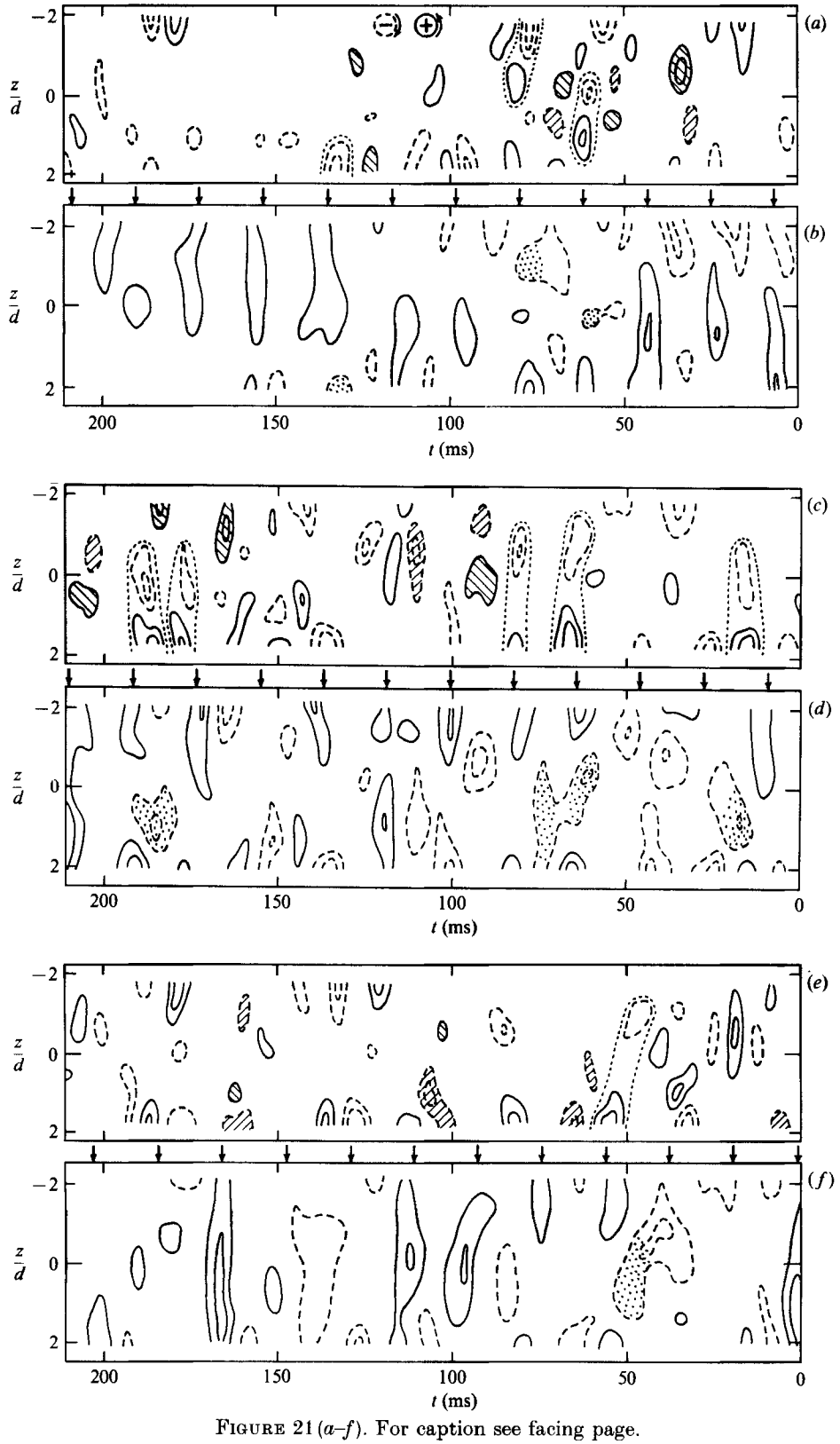

FIGURE 21 (*a–f*). For caption see facing page.

Therefore, it is hard to draw very definite conclusions from the limited information provided by our data. In particular, when higher-velocity contours (and thus rolls) are significantly contorted or even missing, there is no way to distinguish ribs from rolls. Pending more detailed data in a wake, we suggest that, at least, the hatched $\tilde{\omega}_y$ contours are manifestations of ribs. If this is really the case, the strength and size of ribs are not drastically different from those of contorted rolls.

The relatively large scale of longitudinal structure was found by Jimenez *et al.* (1985) in image-enhanced visualization pictures of a plane mixing layer. To date, no quantitative measurements of longitudinal vorticity have been reported in free shear flows, but observations that the cavitation inception in separated mixing layers in water occurs first in streamwise streaky regions (Katz & O'Hern 1986; A. Acosta 1987, private communication) suggest the presence of fairly intense longitudinal vorticity which produces localized low-pressure regions in those cores. Therefore, it may not be unrealistic to regard the $\tilde{\omega}_y$-concentrations of hatched contours in figure 21 (*a*, *c*, *e*) as the signatures of ribs.

6.2. *Some other aspects of ribs*

In this subsection, we add further discussion concerning the longitudinal substructures.

Lasheras *et al.* (1986) found in a low-Reynolds-number mixing layer that concentrated streamwise vorticity was always initiated in the braid by the unstable response of spanwise vortex lines to small three-dimensional perturbations, and suggested that such instability would continue to propagate the three-dimensionality sideways in a manner similar to the 'translative instability' proposed by Pierrehumbert & Widnall (1982). A somewhat similar observation in the very near wake of a circular cylinder was reported by Wei & Smith (1986), who showed that a near-wake free shear instability produced secondary vortices which then evolved into cellular structures. A rough estimation from their pictures (their figures 8 and 9) of the spanwise distance between paired legs of the cellular structure yields $0.4d$–$0.6d$ at $Re_d = 3570$ and 4530. Meanwhile, the distance between paired $\tilde{\omega}_y$ patches (estimated from the hatched contours in figure 21 *a*, *c*, *e*) is roughly $1d$–$2d$. In addition, Wei & Smith's result (their figure 11) shows that the scale of the cellular structures decreases with increasing Reynolds number. Thus, both the scale and spanwise separation of the cellular structures corresponding to our case ($Re_d = 1.3 \times 10^4$), if they occur, should be much smaller than those of the $\tilde{\omega}_y$-patches in figure 21. This comparison suggests that the secondary vortices observed by Wei & Smith in the vicinity of the cylinder could not be directly related to apparent substructures recognized by the present measurement.

As such, it is unclear whether earlier studies which focus on either transition region or low-Reynolds-number case, are relevant to fully turbulent flows. In fact, Wei & Smith observed that the cellular structure of secondary vortices was obscured in high-Reynolds-number cases. Our conjecture is that the vortex stretching in the braid plays a key role in generating ribs, as argued by Corcos & Lin (1984), Hussain (1984) and Lasheras *et al.* (1986); that is, any three-dimensional vorticity perturbation in the braids would be stretched by the intense strain produced by the

---

FIGURE 21. Three sets of simultaneously measured, instantaneous $\tilde{\omega}_y$- and $\tilde{u}$-maps at $x/d = 20$; contour levels of (*a*, *c*, *e*), $\tilde{\omega}_y/S_M = \pm 3$, ± 1.5; contour levels of (*b*, *d*, *f*), $(\tilde{u} - U_c)/U_0 = \pm 0.125$, ± 0.075.

nominally spanwise rolls (see figure 4) and would tend to be organized and aligned in the direction of the principal axis of strain ('the Corcos mechanism'). The ribs thus formed should be subjected to continual stretching along the braid (Lin & Corcos 1984; Neu 1984), and the induction of the ribs may, in turn, distort the rolls primarily in the spanwise direction (Hussain 1984; HH).

Another relevant result recently obtained by Kiya & Matsumura (1988) is that the most significant contribution to the incoherent Reynolds shearing stress in the saddle region (in the near wake of a normal plate) comes from fluctuations with frequencies around one-half of the vortex shedding frequency. In order to explain such a dominant role of the subharmonic component, they propose that ribs in consecutive saddle regions have a staggered arrangement. Let us refer again to figure 21 (a, c, e) and examine the hatched $\tilde{\omega}_y$-concentrations in the timewise direction. We can see some occasions of vorticity patches at a given z being of alternating signs in t; typical examples are three successive pairs of vorticity patches between $t \approx 30$ and 70 ms in figure 21 (a) and two successive ones between $t \approx 90$ and 110 ms in figure 21 (c). These cases correspond to the staggered arrangement of ribs. On the other hand, there is no clear example that shows the streamwise alignment of $\tilde{\omega}_y$-patches. We might therefore conclude that the dominant streamwise arrangement of ribs is a staggered one. However, this is a very tentative conclusion because of the limited number of available examples. Note that flow visualizations of plane mixing layers to date (e.g. Brown & Roshko 1974; Bernal & Roshko 1986) suggest continued streamwise alignment of successive streaky patterns. The dominant spatial arrangement of ribs in a wake needs to be examined further by alternative quantitative measurements which would be required to take into consideration a possible relationship between the substructures (i.e. ribs) on both sides of the wake.

6.3. *Comparison with far-field structures*

The present experiment, which only covers up to $x/d = 40$, might not be totally relevant for discussing the far-field structure of the wake. However, our results (including those of HH) suggest that the spatial behaviour of organized structures in the intermediate wake should bear qualitative resemblance, in many respects, to the one in the far wake. For instance, Browne, Antonia & Bisset (1986) and Antonia *et al.* (1987) find by using temperature fluctuations as a trigger signal that the velocity vector pattern (sliced by an (x, y)-plane) of a heated cylinder wake at $x/d = 420$ is quite similar to that obtained by HH. Thus, comparison of observations in the two regions would help our understanding of the far-field structures as well.

Townsend (1979) suggests that organized structures in the far wake occur as groups, with regular spacing between structures in a group but irregular spacing between groups. Wygnanski *et al.* (1986) and Antonia *et al.* (1987) observe that the far-field structures appear sometimes as an antisymmetric mode (like the Kármán street) and at other times as a symmetric mode. Such trends exist in the instantaneous ω_z-maps at $x/d = 40$ (figure 2*b*; see also figures 1*d–g* in HH). That is, structures occur fairly regularly for some intervals but quite irregularly at others, and the dispersions of transverse displacement and streamwise spacing of individual structures are very large (structures shed from one side of the cylinder often cross the wake centre-plane). Thus, it is not unexpected that the structure groups as well as the two modes of structure arrangement can be locally observed farther downstream.

The present data show that the most probable configuration of three-dimensional structures is a horseshoe-like vortex associated with a low-speed lump of fluid between paired (counter-rotating) $\tilde{\omega}_y$-concentrations, suggesting that they are

formed by the outward kinking of spanwise rolls (see figure 13*a*). This is qualitatively consistent with Mumford's (1983) observation in the far wake that his type-B↑ double rollers (similar to the ω_y-pattern in our figure 13*a*) make a considerably larger contribution than his type-B↓ rollers (similar to figure 13*b*). Note that asymmetric horseshoe-like vortices could be ambigiously recognized as a single roller, as was done by Mumford, because a large difference between the two legs of a horseshoe-like vortex can frequently occur, as discussed in §5.

The transverse structure like Grant's model extending across the wake centreplane has not been detected in the intermediate wake. In this respect, Mumford (1983) carefully discriminated between structures confined to one side of the wake centreplane and those crossing it, and found that the proportion of occurrence of the former structures is considerably larger. Our data (figure 15*a*, *b*) show that a non-negligible amount of $\langle\omega_y\rangle$ is educed at the centreplane ($y = 0$) when triggered by the $\tilde{\omega}_y$-concentrations at $y = 30$ mm, even though the coherence drops off drastically across the centreplane. This suggests that horseshoe-like vortices would occasionally cross the centreplane and encroach into the other side of the wake in farther downstream regions because of the increasing wandering of structures with increasing x. Therefore, it seems that most of the fraction regarded by Mumford as double-sided structures are not closed loops but are the usual horseshoe-like vortices originated from either side.

Of course, vortex interactions (say, cut-and-connect interactions; see Takaki & Hussain 1985) may cause crosslinking to rearrange two horseshoe-type vortex tubes from both sides of the wake into a single transverse vortex loop. However, contrary to suggestions by many (e.g. Roshko 1976; Coles 1982; Savill 1983), we consider that the closed vortex loop across the wake centreplane would be an improbable dominant structure even in the far field, because horseshoe-like vortices may not frequently occur in a symmetric way with respect to the wake centreplane. This claim, of course, must be checked by applying measurement techniques such as ours to the far-field region. Such an effort has been started by Antonia (1987) who has adopted the X-wire rake approach introduced by us (Tso 1983; Hayakawa & Hussain 1985).

7. Concluding remarks

It seems to us that vorticity is the best flow property to observe in the investigation of organized structures in turbulent shear flows (Hussain 1980, 1983; Saffman 1981; Coles 1982). Nevertheless, no attempt at multiplane vorticity measurements, which ought to be used to construct spatial pictures of organized structures, has yet been made. Thus, the present effort is a first (and perhaps ambitious) step. In earlier works, attention was focused on the accurate measurement of vorticity at points in the wall region of boundary-layer flows, and thus the vorticity probe had to be comparable with a viscous length (see, for example, a review article of Wallace 1986), whereas the present technique focuses primarily on capturing the large-scale, spatially correlated vorticity (i.e. coherent vorticity) directly.

With several combinations of X-wire arrays, we achieved partial success in unveiling the three-dimensional nature of dominant, large-scale organized motions in the intermediate region of a circular cylinder wake. Our results unambiguously demonstrate that significant three-dimensionality occurs in the moderately near field of the nominally two-dimensional flow. Both spatial correlation and phase-aligned ensemble averaging of spanwise vorticity show that the typical spanwise extent of

two-dimensionality of the primary vortices, i.e. rolls, is comparable with the local half-width of the wake. The strong three-dimensionality was further confirmed by transverse vorticity measurements. There are frequent concentrations of transverse vorticity with scales and strengths of the order of the spanwise vorticity. Instantaneous velocity and vorticity maps, as well as ensemble-averaged transverse vorticities in either one or (simultaneously) two (x, z)-planes, indicate that the dominant configuration of distorted rolls is a horseshoe-like vortex inclined at an angle of about 30° to the y-axis. In the transverse vorticity maps, we find apparent signatures of the longitudinal coherent substructures, i.e. ribs; the presence of the ribs in the wake has been inferred by Cantwell & Coles (1983) and HH from detailed coherent and incoherent turbulence properties obtained by a two-dimensional cut of the wake. However, the evidence presented here is not satisfactory owing to the limitation of the experimental technique by which a rigorous discrimination between distorted rolls and ribs could not be made.

In spite of the new quantitative information obtained by the present study, our understanding of the structure details of the plane wake in the three-dimensional space is still far from complete. For instance, how does a roll on one side of the wake interact with one on the opposite side when they are distorted in the spanwise direction? What is the dominant spanwise arrangement of ribs? What kind of interaction might occur between the ribs across the wake centreplane? These fundamental questions could be answered in future work which would require simultaneous measurements of spanwise and streamwise vorticities, perhaps combined with numerical simulation. A promising alternative approach may be a parallel study of two (apparently) extreme cases: (1) a wake behind an artificially excited body (to give minimal spatial jitter of shed vortices); and (2) a porous-plate wake without initial vortex shedding. Such an effort would be of considerable help in answering the above questions and also in resolving the persistent controversy regarding the generation mechanism and geometry of dominant coherent structures in a far-field wake.

The present experiment was done when M. H. stayed in the University of Houston as a visiting researcher during 1982–84. We are grateful to Drs S. J. Kleis and H. S. Husain and Mr J. E. Bridges for their support in experiment and data analyses. M. H. would like to thank Professors Y. Kobashi and M. Kiya for helpful discussion in preparing the initial draft of the paper, and also Professor S. Iida, Dr M. Ichijo and Mr Y. Nozaki for continuous encouragement. This research was supported by the Office of Naval Research under grant N00014-89-J-1361 and the Department of Energy grant DE-FG05-88ER13839.

REFERENCES

ANTONIA, R. A. 1987 In *Proc. 2nd Symp. on Transport Phenomena in Turbulent Flows* p. 339. Tokyo University.

ANTONIA, R. A., BROWNE, L. W. B., BISSET, D. K. & FULACHIER, L. 1987 *J. Fluid Mech.* **184**, 423.

ARMSTRONG, B. G., BARNES, F. H. & GRANT, I. 1987 *Phys. Fluids* **30**, 19.

BERNAL, L. P. & ROSHKO, A. 1986 *J. Fluid Mech.* **170**, 499.

BONNET, J. P., DELVILLE, J. & GAREM, H. 1986 *Exp. Fluids* **4**, 189.

BREIDENTHAL, R. 1980 *Phys. Fluids* **23**, 1929.

BROWAND, F. K. & TROUTT, T. R. 1985 *J. Fluid Mech.* **158**, 489.

BROWN, G. & ROSHKO, A. 1974 *J. Fluid Mech.* **64**, 775.

BROWNE, L. W. B., ANTONIA, R. A. & BISSET, D. K. 1986 *Phys. Fluids* **29**, 3612.

CANTWELL, B. & COLES, D. 1983 *J. Fluid Mech.* **136**, 321.

CIMBALA, J. M., NAGIB, H. M. & ROSHKO, A. 1988 *J. Fluid Mech.* **190**, 265.

COLES, D. 1982 In *Surveys in Fluid Mechanics* (ed. R. Narashima & S. M. Deshpande), p. 17. Ind. Acad. Sci.

COLES, D. 1984 In *Turbulence and Chaotic Phenomena in Fluids* (ed. T. Tatsumi), p. 397. North-Holland.

CORCOS, G. M. & LIN, S. J. 1984 *J. Fluid Mech.* **139**, 67.

GRANT, H. L. 1958 *J. Fluid Mech.* **4**, 149.

GRINSTEIN, F. F., ORAN, E. & HUSSAIN, A. K. M. F. 1987 In *Proc. 6th Symp. on Turbulent Shear Flows*. Toulouse. Université Paul Sabatier.

HAYAKAWA, M. & HUSSAIN, A. K. M. F. 1985 In *Proc. 5th Symp. on Turbulent Shear Flows*, p. 4.33. Cornell University.

HAYAKAWA, M. & HUSSAIN, A. K. M. F. 1986 In *Proc. 3rd Asian Congr. Fluid Mech.* (ed. T. Matsui), p. 206. H. Sato.

HEAD, M. R. & BANDYOPADHYAY, P. 1981 *J. Fluid Mech.* **107**, 297.

HUSSAIN, A. K. M. F. 1980 In *Role of Coherent Structures in Modelling Turbulence and Mixing* (ed. J. Jimenez). Lecture Notes in Physics, vol. 136, p. 252. Springer.

HUSSAIN, A. K. M. F. 1983 *Phys. Fluids* **26**, 2816.

HUSSAIN, A. K. M. F. 1984 In *Turbulence and Chaotic Phenomena in Fluids* (ed. T. Tatsumi), p. 453. North-Holland.

HUSSAIN, A. K. M. F. 1986 *J. Fluid Mech.* **173**, 303.

HUSSAIN, A. K. M. F. & HAYAKAWA, M. 1987 *J. Fluid Mech.* **180**, 193 (referred to as HH).

HUSSAIN, A. K. M. F. & ZAMAN, K. B. M. Q. 1981 *J. Fluid Mech.* **110**, 39.

HUSSAIN, A. K. M. F. & ZAMAN, K. B. M. Q. 1982 *Rep.* FM-14. University of Houston; see also *J. Fluid Mech.* **159**, 85 (1985).

JIMENEZ, J. 1987 *J. Fluid Mech.* **178**, 177.

JIMENEZ, J., COGOLLOS, M. & BERNAL, L. P. 1985 *J. Fluid Mech.* **152**, 125.

KATZ, K. & O'HERN, T. J. 1986 *Trans. ASME* I: *J. Fluids Engng* **108**, 373.

KIDA, S. 1982 *J. Fluid Mech.* **122**, 487.

KIYA, M. & MATSUMURA, M. 1985 *Bull. JSME* **28**, 2617.

KIYA, M. & MATSUMURA, M. 1988 *J. Fluid Mech.* **190**, 343.

LARUE, J. C. & LIBBY, P. A. 1974 *Phys. Fluids* **17**, 873.

LASHERAS, J. C., CHO, J. S. & MAXWORTHY, T. 1986 *J. Fluid Mech.* **172**, 231.

LIN, S. J. & CORCOS, G. M. 1984 *J. Fluid Mech.* **141**, 139.

MATSUI, T. 1982 In *Surveys in Fluid Mechanics* (ed. R. Narashima & S. M. Deshpande), p. 145. Ind. Acad. Sci.

MATSUI, T. & OKUDE, M. 1981 In *Proc. 7th Symp. on Turbulence*, p. 303. University of Missouri-Rolla.

MEIRON, D. I., SAFFMAN, P. G. & SCHATZMAN, J. C. 1984 *J. Fluid Mech.* **147**, 187.

METCALFE, R. W., HUSSAIN, A. K. M. F., MENON, S. & HAYAKAWA, M. 1987*a* In *Turbulent Shear Flows*, Vol. **5** (ed. F. Durst *et al.*), **110**. Springer.

METCALFE, R. W., ORSZAG, S. A., BRACHET, M. E., MENON, S. & RILLY, J. J. 1987*b* *J. Fluid Mech.* **184**, 207.

MOIN, P. & KIM, J. 1985 *J. Fluid Mech*, **155**, 441.

MUMFORD, J. C. 1983 *J. Fluid Mech.* **137**, 447.

NEU, J. C. 1984 *J. Fluid Mech.* **143**, 253.

PIERREHUMBERT, R. T. & WIDNALL, S. E. 1982 *J. Fluid Mech.* **114**, 59.

ROBINSON, A. C. & SAFFMAN, P. G. 1982 *J. Fluid Mech.* **125**, 411.

ROGERS, M. M. & MOIN, P. 1987 *J. Fluid Mech.* **176**, 33.

ROSHKO, A. 1976 *AIAA J.* **14**, 1349.

SAFFMAN, P. G. 1981 *J. Fluid Mech.* **106**, 49.

SAVILL, A. M. 1983 In *Structure of Complex Turbulent Shear Flows* (ed. R. Dumas & L. Fulachier), p. 185. Springer.

TAKAKI, R. & HUSAAIN, A. K. M. F. 1985 In *Proc. 5th Symp. Turbulent Shear Flows,* p. 3.19. Cornell University.

TANEDA, S. 1959 *J. Phys. Soc. Japan* **14**, 843.

TOWNSEND, A. A. 1956 *The Structure of Turbulent Shear Flow.* Cambridge University Press.

TOWNSEND, A. A. 1979 *J. Fluid Mech.* **95**, 515.

TSO, J. 1983 Coherent structures in a fully-developed turbulent axisymmetric jet. Ph.D. thesis, The Johns Hopkins University.

TSO, J. & HUSSAIN, F. 1989 *J. Fluid Mech.* **202**, 225.

WALLACE, J. M. 1986 *Exp. Fluids* **4**, 61.

WEI, T. & SMITH, C. R. 1986 *J. Fluid Mech.* **169**, 513.

WYGNANSKI, I., CHAMPAGNE, F. & MARASLI, B. 1986 *J. Fluid Mech.* **168**, 31.

WYGNANSKI, I., OSTER, D., FIEDLER, H. & DZIOMBA, B. 1979 *J. Fluid Mech.* **93**, 325.